Journal of Mechatronics, Electrical Power, and Vehicular Technology 17 (2026) 38-53

Journal of Mechatronics, Electrical Power, and Vehicular Technology

e-ISSN: 2088-6985
p-ISSN: 2087-3379

mev.brin.go.id

Response surface methodology to optimize aerial mapping electric UAV preliminary design and static stability analysis

Prytha Virgiawan Lesalli [a], Tresna Priyana Soemardi [a, *], Lilis Mariani [a, b]

[a] *Department of Mechanical Engineering, Universitas Indonesia*
Depok, 16425, Indonesia

[b] *Aeronautics and Space Research Organization, National Research and Innovation Agency*
Bogor Regency, 16350, Indonesia

Abstract

This study addresses the need for efficient aerodynamic design in fixed-wing unmanned aerial vehicles (UAVs) for aerial mapping applications, where flight stability and cruising performance are critical. The research aims to optimize wing geometry parameters to achieve the desired cruising speed while minimizing drag and ensuring static stability. The methodology integrates conceptual and preliminary design approaches, followed by aerodynamic simulations using XFLR-5 with the vortex lattice methodology (VLM-2). Three design variables, winglet length, cant angle, and twist angle, are systematically varied, and the response surface methodology (RSM) is employed to model and optimize their effects on lift, drag, and airspeed. The optimization results indicate that the optimal configuration achieves a cruising speed of 16.8 m/s with improved lift characteristics (CL ≈ 0.48) and controlled drag (CD ≈ 0.022). Further analysis confirms that the optimized UAV satisfies longitudinal, lateral, and directional static stability criteria under various control surface deflections. In conclusion, the integration of RSM with aerodynamic simulation provides an effective and systematic framework for enhancing the UAV performance and stability, particularly in aerial mapping missions.

Keywords: aerial mapping UAV design; fixed-wing UAV design optimization; UAV static stability analysis.

I. Introduction

Unmanned aerial vehicles (UAVs) are rapidly transforming aerial mapping operations, offering cost-effective and versatile platforms for acquiring high-resolution imagery and spatial data. These aircraft, operated wirelessly or autonomously and guided by global positioning system (GPS) with gyro stabilization, provide surveyors and spatial data analysts with powerful tools for efficient project examination. Fixed-wing UAVs offer distinct advantages for aerial mapping, particularly in surveying large, open areas. Their increased endurance, lower maintenance costs, and inherent suitability for georeferencing make them a compelling choice for enhanced efficiency and speed [1][2][3]. The diverse requirements of various missions necessitate different UAV models. To select the most suitable UAV for a specific task, we must consider both the UAV's conceptual design and its design and requirements objectives (DRO) in the conceptual design phase.

The successful deployment of fixed-wing UAVs for aerial mapping hinges on a robust design process that encompasses conceptual, preliminary, and detailed

* Corresponding Author. tsoemardi@eng.ui.ac.id (T. P. Soemardi)

https://doi.org/10.55981/j.mev.2026.1230

Received 13 October 2025; revised 18 February 2026; accepted 7 April 2026; available online 25 June 2026

How to Cite: P. V. Lesalli *et al.*, "Response surface methodology to optimize aerial mapping electric UAV preliminary design and static stability analysis," *Journal of Mechatronics, Electrical Power, and Vehicular Technology*, vol. 17, no. 1, pp. 38-53, July, 2026.

design phases. The conceptual design phase establishes the design and requirements objectives (DRO), initial geometry, and basic parameters [4]. In the crucial preliminary design phase, determining the wing reference area and engine thrust, guided by the DRO and performance requirements through techniques like National Aeronautics and Space Administration (NASA) 'Matching Plot' [4][5], is essential. This phase also includes weight and balance estimation, encompassing takeoff gross weight, fuel weight, and empty weight, which includes the airframe and avionics [6][7]. Critically, all steps in the preliminary design are intertwined with the aerodynamic and stability characteristics of the UAV. Static stability, the aircraft's inherent ability to resist disturbances and return to equilibrium, is paramount for safe and predictable flight, especially during automated aerial mapping missions. Analyzing this stability involves considering the forces and moments acting on the aircraft, with the center of gravity as a key reference point. XFLR-5 software, a widely-used software employing the lifting line theory (LLT) and vortex lattice method (VLM) methods, facilitates stability analysis by providing rapid approximations and enabling extensive testing of wing and tail parameter variations [8][9][10], several studies have also used these methods to optimize the design by adding and studying the wing performance effect using wing geometry and winglet variation [11][12]. This is vital because wing parameters are interconnected, and changes in one can significantly impact overall performance, requiring a global approach to control [13]. Furthermore, the accuracy of XFLR-5 in predicting aerodynamic characteristics has been validated through comparisons with computational fluid dynamics (CFD) simulations and experimental testing [14][15][16].

Recognizing the computational efficiency of the vortex lattice method (VLM) within XFLR-5, this research employs the response surface methodology (RSM) to optimize the preliminary design of a fixed-wing aerial mapping UAV. RSM is a statistical technique used to model the relationship between multiple design variables and system responses, enabling efficient exploration of complex design spaces [17]. It has been widely applied in engineering optimization to identify optimal parameter configurations and improve system performance [18]. In manufacturing and process engineering, RSM has demonstrated strong capability in capturing nonlinear interactions between variables and constructing predictive models based on experimental or simulation data [19], while also being effective in solving multi-objective optimization problems involving competing performance criteria [20].

More recently, RSM has been increasingly applied in aerospace design. For instance, it has been used to model the relationship between structural parameters and UAV endurance, achieving significant improvements in flight performance through optimized configurations [21][22]. In addition, RSM-based optimization of aircraft wing structures has demonstrated its capability to reduce structural weight and stress while maintaining performance constraints, highlighting its efficiency in reducing computational cost during design iterations [21]. These advancements demonstrate that RSM is a reliable and efficient approach for handling multidisciplinary design variables in aircraft preliminary design, particularly for improving aerodynamic performance, stability characteristics, and overall system efficiency in UAV applications [22].

This paper is organized as follows: Section I provides a detailed review of relevant literature on UAV design optimization, stability analysis, and the application of RSM in aerospace engineering. Section II outlines the methodology employed, including the RSM approach, XFLR-5 simulations, and stability criteria. Section III presents the optimization results, and finally, Section IV discusses the findings and their implications for aerial mapping UAV design. This paper also includes a summary of key contributions and future research directions.

II. Materials and Methods

The research begins with determining the conceptual design, followed by a preliminary design to obtain power and wing loading estimations. The value of power and wing loading estimation is used to design the wing and tail reference. Continued analysis of aerodynamic characteristics in the form of lift, drag, and speed requirements on wing geometry variations was determined by using XFLR-5 software. These variations will be optimized using the response surface methodology. The optimum geometry results will be analyzed for stability characteristics with trim variations on each control surface to determine whether the aircraft has static stability and the effect of control surface deflection on the moment coefficient acting on the aircraft.

A. UAV conceptual design

Fixed-wing aerial mapping UAVs advance in flight endurance and can cover larger areas in one flight also applied successfully for a variety of environmental or specific applications [3][23][24]. The flight path or flight mission for aerial mapping with survey grid mode is commonly used for an aerial mapping UAV mission

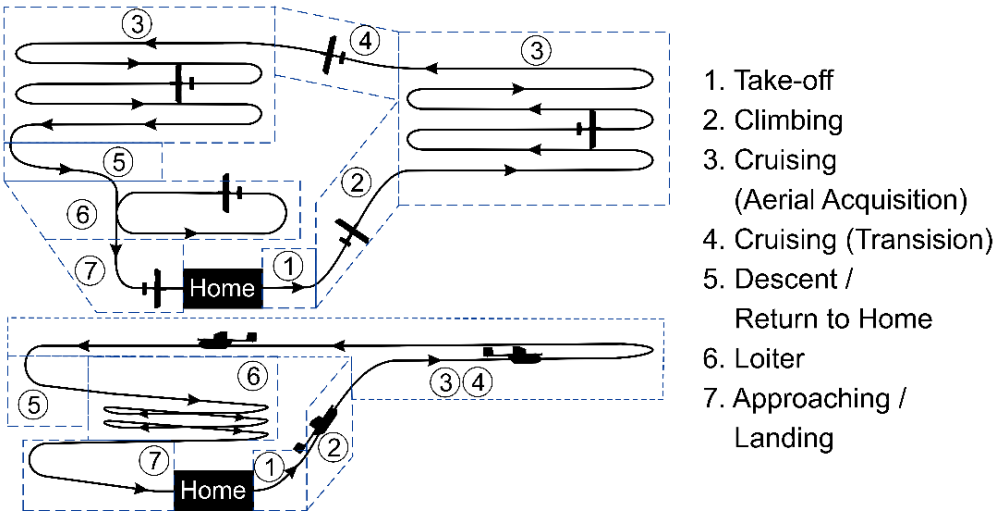

Figure 1. Typical mission for aerial mapping.

consisting of several main phases, such as: take- off, climb, cruising, loiter, approach, and landing [5][25][26]. As shown in Figure 1, after UAVs take off and climb to a determined altitude, the flight path during photogrammetry acquisition uses several parallel line paths to survey some areas. If the aircraft surveys more than one area of interest, the aircraft will transition to move to another parallel line path.

A small UAV with a 1900 mm wingspan is used as a benchmark, one of the popular aircraft units in an aerial mapping company, to carry an RGB camera for the purpose of collecting aerial images. Figure 1 is also used as a common mission to collect the aerial data. The cruising phase (aerial acquisition) is a very important phase because it affects the quality of acquired data. The cruising phase is used as a parameter to decide the maximum altitude that can be acquired by the aircraft, also used as a reference for cruising speed, which will be used as design requirements and objectives.

One of the important parameters is flight speed; flight speed can cause altitude or Z errors, which is possibly due to low image quality and too long exposure times because of faster flight speed [3][27]. This research uses data telemetry logs from 31 flights with 332 lines for aerial mapping operated with Ground Sample Distance 2-4 cm at an altitude of 80-200 m above the ground level as a benchmark for flight speed requirements according to airspeed in that data.

B. UAV preliminary design

The preliminary design sets the baseline for the UAV's structure and configuration, including the airfoil, wing geometry, and tail design. These elements directly influence the UAV's aerodynamic characteristics, which are critical for performance and stability. Performance analysis evaluates how well the UAV meets its operational requirements, such as lift-to-drag ratio, cruising speed, stall speed, and maximum speed [5]. It ensures that the preliminary design can achieve the desired flight characteristics and efficiency [28][29]. Stability analysis examines the UAV's ability to maintain controlled and balanced flight under various conditions. It focuses on factors to ensure the UAV remains stable during flight [24][30]. In this research, the UAV preliminary design involves steps such as wing and power loading estimation, wing tail design, mass distribution, wing optimization, and static stability analysis using VLM2 by XFLR-5 software and response surface methodology.

C. Wing and power loading estimation

The crucial step in the aircraft preliminary design phase is to determine wing reference area (S) and engine thrust (T) for a jet engine or engine power (P) for a propeller-driven engine. By using a "matching plot" to obtain power loading [W/P] and wing loading [W/S], this approximation depends on the initial flight performance parameter, followed by deriving an equation for each performance requirement with a power and wing loading function [15][17]. Requirements functions that are used to plot, such as:

- Stall speed, as shown in equation (1), is the minimum required airspeed that can cause a stall.

$$\left[\frac{W}{S}\right]_S = \frac{1}{2}\rho v_s^2 C_{Lmax} \quad (1)$$

- Maximum speed $\left[\left[\frac{W}{P}\right]_{Vmax}\right]$, as shown in equation (2), is the weight per power requirement for maximum aircraft speed.

$$\left[\frac{W}{P}\right]_{Vmax} = \frac{\eta_p\,(550)}{0.5\,\rho\,v^3{}_{max}\,C_{D0}\frac{1}{[w/s]} + \frac{2\,K}{\rho\,\sigma\,v_{max}}\left[\frac{W}{s}\right]} \quad (2)$$

- Take-off run, as shown in equation (3), is the requirement for maximum take-off run.

Table 1.
Typical values for several parameter UAV.

Parameter	Typical values	Name
C_{D0}	0.02-0.03	Zero-lift drag coefficient
Ar	5-20	Wing aspect ratio
C_{Lc}	0.2-0.5	Cruise lift coefficient
C_{Lmax}	1.2-1.6	Lift coefficient maximum
e	0.6-0.9	Oswald number
η_P	0.6-0.8	Prop efficiency
$(C_L/C_D)_{max}$	6-10	Maximum lift-to-drag ratio

$$\left[\frac{W}{P}\right]_{Sto} = \frac{1-\exp\left(0.6\rho\, g C_{DG}\, Sto \frac{1}{\left[\frac{W}{S}\right]}\right)}{\mu-\left[\mu+\frac{C_{DG}}{C_{LR}}\right]\left[exp(0.6\rho\, g C_{DG}\, Sto \frac{1}{\left[\frac{W}{S}\right]})\right]} \frac{\eta p}{Vto}(550) \quad (3)$$

- Rate of climb, as shown in equation (4), is the requirement for rate of climb ability.

$$\left[\frac{W}{P}\right]_{Roc} = \frac{1(550)}{\frac{Roc}{\eta p}+\sqrt{\frac{2}{2\sqrt{\frac{3C_{D0}}{K}}}\left[\frac{W}{S}\right]\left[\frac{1.155}{(L/D)max\,\eta p}\right]}} \quad (4)$$

- Ceiling $\left[\left[\frac{W}{P}\right]_{hc}\right]$, as shown in equation (5), is the weight per power requirement for aircraft at the service ceiling.

$$\left[\frac{W}{P}\right]_{hc} = \frac{\sigma_c(550)}{\frac{Roc_c}{\eta_P}+\sqrt{\frac{2}{\rho\sqrt{\frac{3C_{D0}}{K}}}\left[\frac{W}{S}\right]\left(\frac{1.155}{(L/D)max\,\eta_P}\right)}} \quad (5)$$

- Absolute ceiling $\left[\left[\frac{W}{P}\right]_{ac}\right]$, as shown in equation (6), is the weight per power requirement for aircraft at the absolute ceiling.

$$\left[\frac{W}{P}\right]_{ac} = \frac{\sigma_{Ac}(550)}{\sqrt{\frac{2}{\rho_{Ac}\sqrt{\frac{3C_{D0}}{K}}}\left[\frac{W}{S}\right]\left(\frac{1.155}{(L/D)max\,\eta_P}\right)}} \quad (6)$$

- Equation (1) – (6) are plotted into a matching chart to consider power and wing loading. Using equation (7) to equation (8) can be estimated.

$$S = Wto/\left[\frac{W}{S}\right] \quad (7)$$

$$P = Wto/\left[\frac{W}{P}\right] \quad (8)$$

where ρ is the air density, v is velocity, C_{Lmax} is the maximum lift coefficient, η_p is propeller efficiency, C_{D0} is the zero-lift drag coefficient, K is the induced drag factor, μ runway friction coefficient, C_{DG} is the ground drag coefficient, C_{LR} is the obtaining lift coefficient, g is gravitational acceleration, Sto is short take-off length, Roc is the rate of climb, $(L/D)_{max}$ is the lift maximum drag ratio, Roc_c is the rate of climb at service ceiling, σ_{Ac} is the air density ratio at the service ceiling, ρ_{AC} is the air density at the service ceiling and Wto is the UAV's total weight. Table 1 is used for typical value parameters [5].

D. Tail design

This step is intended to consider the tail area as shown in equation (9) to equation (10) with vertical stabilizer area S_v by vertical tail disposition X_v, vertical tail volume coefficient $\bar{V}_v$, horizontal stabilizer area S_h by horizontal tail disposition X_h, horizontal tail volume coefficient $\bar{V}_h$, $\bar{C}$ is a wing mean aerodynamic chord and b is a wing span [31][32].

$$S_h = \frac{\bar{V}_h\, S\, \bar{C}}{X_h} \quad (9)$$

$$S_v = \frac{\bar{V}_v\, S\, b}{X_v} \quad (10)$$

E. Static stability and trim analysis

Stability, in the context of flight dynamics, refers to a system's inherent ability to return to equilibrium after a disturbance. Static stability specifically concerns the initial tendency of a vehicle to revert to its original state. Illustrations of moments act while UAV flight are shown in Figure 2.

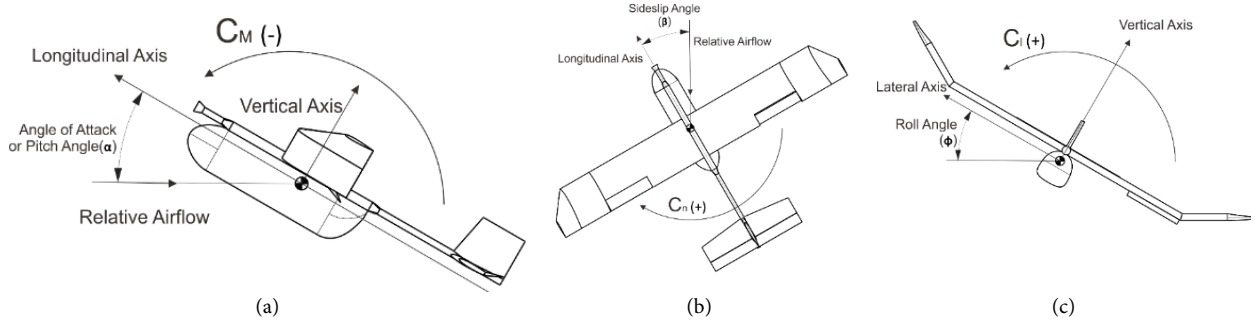

(a) (b) (c)

Figure 2. UAV coefficient moment (a) pitching; (b) yawing; (c) rolling.

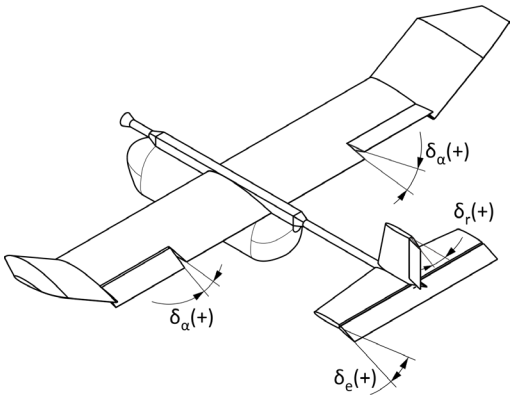

Figure 3. Control surfaces trim.

The pitching curve moment is used to considering longitudinal static stability characteristic of an aircraft. Figure 2 (a) is an elaborate angle of attack α, with C_M, pitching moment coefficient obtained from equation (11) to equation (12) with M for a moment, ρ as air density, v as relative air-speed, S as wing area, and $\bar{c}$ as the wing's mean aerodynamic chord. On the basis of simple analysis, a negative gradient $C_{M\alpha}$ or $\frac{dC_M}{d\alpha} < 0$ is categorized as static stability [9].

$$C_M = \frac{M}{\frac{1}{2}\rho v^2 S\bar{C}} \tag{11}$$

$$C_{M\alpha} = \frac{dC_M}{d\alpha} \tag{12}$$

To achieve lateral stability, the airplane must develop a yawing moment C_n that will restore the airplane to its equilibrium state. When the aircraft is flying, and it is disturbed from the equilibrium condition with a sideslip angle β, The airplane should have a rotational tendency to return to its equilibrium condition, defined in equation (13) and Figure 2 (b). In lateral stability, this condition can be written as $C_{n\beta} > 0$ [9].

$$C_{n\beta} = \frac{dC_n}{d\beta} \tag{13}$$

The airplane exhibits static roll or directional stability when a corrective force is generated to bring it back to a level wing position after it is displaced from this position. This corrective rolling moment C_l can be demonstrated to be a result of the sideslip angle, sideslip angle depicted in Figure 2 (b), and rolling moment, Figure 2 (c). The requirement for stability described in equation (14) is that $C_{l\beta} < 0$. The airplane's tendency to roll during a sideslip is determined by the interplay of wing dihedral, wing sweep, the wing's location relative to the fuselage, and the effectiveness of the vertical tail [9].

$$C_{l\beta} = \frac{dC_l}{d\beta} \tag{14}$$

For an aircraft to maintain steady flight, the sum of forces and moments acting on it must be zero. This condition, known as equilibrium or trim, ensures that the aircraft experiences no acceleration. Conversely, deviations from equilibrium result in translational or rotational accelerations. Control surface deflections or trim is shown in Figure 3, where δ_e is elevator deflection, δ_α is aileron deflection and δ_r is rudder deflection.

Trim control power affects the moment coefficient value by trimming the control surface, as described in the equation (15) to equation (18).

- Elevator control power affects the pitching moment coefficient ($C_{M\delta_e}$):

$$C_{M\delta_e} = \frac{dC_M}{d\delta_e} \tag{15}$$

- Rudder control power affects the yaw coefficient moment ($C_{n\delta_r}$):

$$C_{n\delta_r} = \frac{dC_n}{d\delta_r} \tag{16}$$

- Rudder control power affects the roll coefficient moment ($C_{l\delta_r}$):

$$C_{l\delta_r} = \frac{dC_l}{d\delta_r} \tag{17}$$

- Aileron control power affects the roll coefficient moment ($C_{l\delta_a}$):

$$C_{l\delta_a} = \frac{dC_l}{d\delta_a} \tag{18}$$

In this research, all moment coefficients and aerodynamic characteristics were obtained using the XFLR-5 software.

F. Mass distribution

The coefficient of moment is also affected by the center of gravity (CG) location. CG is concentrated on all weights distributed in the aircraft. CG location in X, Y, and Z coordinates from the relative datum can be estimated using equation (19) – (21). Here m_i denotes the mass of the *i-th component*, x_i, y_i, and z_i represent the corresponding position coordinates relative to the reference datum, and $i = 1, 2, 3, \ldots, n$ indicates each component contributing to the total mass of the UAV [6][7].

$$\bar{x}_{CG} = \frac{\sum_{i=1}^{n} m_i \bar{x}_i}{\sum_{i=1}^{n} m_i} \tag{19}$$

$$\bar{y}_{CG} = \frac{\sum_{i=1}^{n} m_i \bar{y}_i}{\sum_{i=1}^{n} m_i} \tag{20}$$

$$\bar{z}_{CG} = \frac{\sum_{i=1}^{n} m_i \bar{z}_i}{\sum_{i=1}^{n} m_i} \tag{21}$$

To obtain the center of gravity at 25 % of the mean aerodynamic chord length, the location of some aircraft components is iterated until the CG is located at the desired place [30].

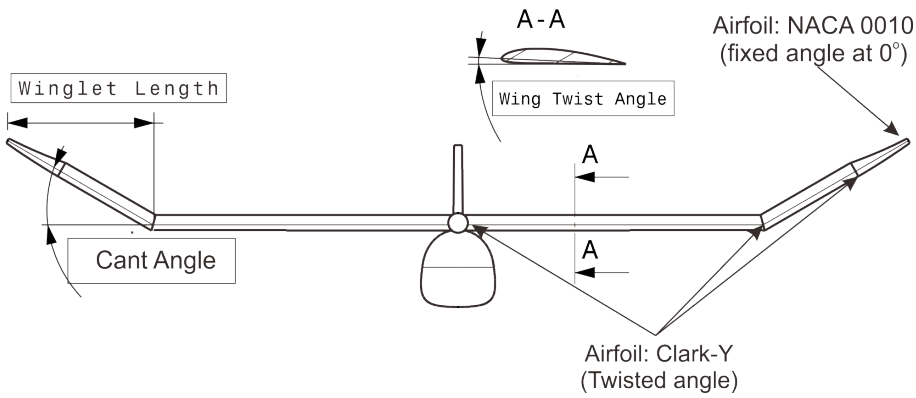

Figure 4. Wing independent variable.

G. Winglet optimization

This research varies three input independent variables, including winglet length, winglet cant angle, and wing twist angle or angle of incidence. The parameter used as an independent variable is shown in Figure 4 and defined in Table 2. The output of this optimization is to consider the wing with the lowest drag and highest lift, and have a specified cruising speed or airspeed based on the reference benchmark. Winglet optimization can improve efficiency and improve the wing UAV for better roll stability, control, and a better endurance by affecting lift, drag, and moment coefficient [33][34][35].

For the purpose of optimization, the response surface methodology is conducted to obtain the optimum output from varying independent variables. Response surface methodology is a statistical and mathematical method used to model the relationship between multiple variables and the responses they produce. Design of experiment (DoE) was used to determine the causal relationship among the different experimental parameters, ranging from the dependence to the interaction between them [20].

III. Results and Discussions

A. Conceptual design

The UAV design incorporates flight speed requirements based on data from 31 aerial mapping flights contains 332 lines. Figure 5 illustrates the distribution of cruising speeds obtained from 31 flight datasets. The data indicate an average cruising speed of 16.8 m/s with a relatively small standard deviation, confirming the consistency of operational conditions. This value is therefore selected as the design target for the UAV optimization process.

Table 3 describes design requirements and objectives. Aircraft objectives can fly until 1100 ft above sea level, making this aircraft capable to capture image at GSD 4 cm up to 150 m ground elevation according to benchmark data. The 1700 mm wingspan is shorter than the benchmark, that have 1900 mm wingspan. Total weight and payload are estimated by calculating the total weight of the common component that is used as an aerial mapping instrument and its parts.

For aerial mapping purposes, this research adopts a configuration consisting of a high wing, rectangular wing, conventional tail, single tail boom, and a tractor single-propeller electric propulsion. The high-wing configuration provides inherent lateral stability and improved ground clearance, which are advantageous for take-off and landing operations in unprepared areas. It also enhances downward visibility, which is essential for aerial mapping missions [32]. A rectangular wing planform is selected due to its geometric simplicity and ease of manufacturing, as well as its predictable

Table 2.
Wing independent variable.

Parameters	Value
Winglet length (mm)	250.351; 257.758; 278.542; 287.939
Cant angle (deg)	0; 10; 20; 30
Twist angle (deg)	0; 1; 2; 3; 4; 5

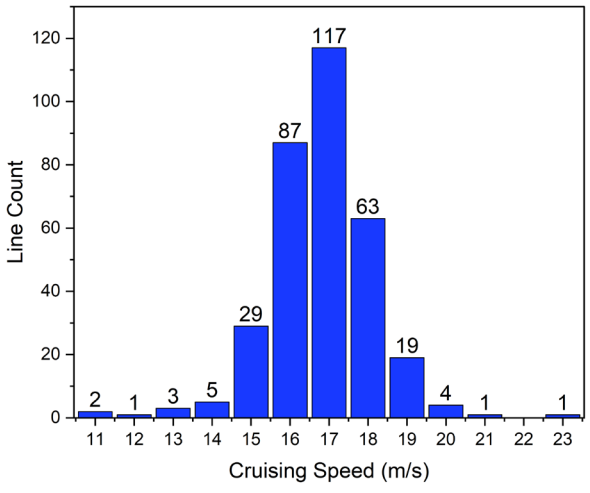

Figure 5. T-log data cruising speed diagram.

Table 3.
Design requirements of objectives.

Parameter	Requirements
Cruising speed	16.8 m/s
Absolute ceiling	1100 ft
Wing span	1700 mm
MTOW or WTO	3 kg
Purposes	Aerial mapping
Payload	829 g total weight for battery and camera

aerodynamic characteristics in low-speed flight regimes, making it suitable for small UAV operations [10][32].

The conventional tail configuration offers stable and well-understood longitudinal and directional control characteristics, facilitating reliable flight behavior and simplifying the design process [31][32]. The use of a single-tail boom reduces structural complexity and overall weight compared to twin-boom configurations, while still maintaining adequate structural integrity for lightweight UAV platforms [31][36]. Furthermore, a tractor single-propeller configuration powered by an electric motor is selected due to its higher propulsion efficiency and reduced aerodynamic interference with empennage surfaces [37]. This configuration also minimizes vibration levels, which is beneficial for improving image quality in aerial mapping applications [38][39]. In addition, electric propulsion systems provide low noise, high reliability, and operational simplicity, making them well-suited for small UAV missions [5][40].

Initial parameters are determined based on Table 4 and subsequently substituted into the governing equations to generate the matching plot for preliminary sizing. These parameters represent key design inputs such as wing loading, power loading, and aerodynamic coefficients required to establish the design space. The matching plot is then used to identify feasible design regions that satisfy multiple performance constraints simultaneously.

The selection of these parameters is based on the design requirements and objectives (DRO), including mission-specific criteria such as cruising speed and operating altitude. These DRO parameters play a critical role in defining the performance constraints, ensuring that the resulting design configuration meets the operational requirements of the aerial mapping mission.

B. Power and wing loading estimation

Table 4 presents the initial design parameters used in the preliminary design phase to construct the matching plot for wing loading and power loading estimation. These parameters include aerodynamic coefficients, flight performance requirements, and environmental conditions derived from the design and requirements objectives (DRO). The selected values, such as cruising speed, air density ratio, lift coefficients, and drag coefficients, serve as key inputs for evaluating performance constraints, including stall speed, rate of climb, take-off distance, and ceiling. By incorporating these parameters into the governing equations, the matching plot can be generated to identify the feasible design region. This table, therefore, plays a critical role in ensuring that the selected UAV configuration satisfies all performance requirements simultaneously.

By utilizing the functions equation (1) to equation (6), a matching plot was generated, as shown in Figure 6. The acceptable region in this plot provides the optimal values for wing loading $[W/S]$ = 9 and

Table 4.
Initial design parameters.

Parameters	Symbol	Value	Units	Parameters	Symbol	Value	Units
C_D 0 lift	C_{D0}	0.025		ρ to ρ_0 ratio	σ	0.91511	
Aspect ratio	Ar	7.27272		Rate of climb	Roc	1050	fpm
C_L cruise	C_{Lc}	0.398		Rate of climb ceiling	Roc_c	1000	fpm
C_L maximum	$C_{L\,max}$	1.58		Absolute ceiling	Ca	11000	ft
Oswald number	e	0.8		Ca air density	ρ_{Ca}	0.00164	
Propeller efficiency	ɲ	0.8		ρ_{Ca} to ρ_0 ratio	σ_{Ca}	0.689896	
$[C_L/C_D]$ max	$[C_L/C_D]_{max}$	1.36		Lift coefficient TO	C_{Lto}	0.3	
Cruising speed	V	55.1	fps	Drag coef TO	C_{Dto}	0.02992	
Service ceiling	hc	3000	ft	Ground friction	μ	0	
Stall speed	Vs	32	fps	Drag coef Gnd	C_{Dg}	0.02992	
Induced drag factor	K	0.054688		C_L at ground	C_{Lg}	1.30578	
Max speed	V_{max}	100	fps	Take off run	Sto	38	ft
Ceiling air density	ρ	0.00217	Slug/ft^3	Take off speed	V_{To}	40	fps
Sea-level air density	ρ_0	0.00237	Slug/ft^3	C_L rotate	C_{Lr}	0.95	

weight-to-weight ratio $[W/P] = 1.621238$. A wing loading of 9 and a thrust-to-weight ratio of 1.621238 were chosen as the design parameters.

Figure 6 presents the matching plot used to determine the feasible design region based on multiple performance constraints, including stall speed, climb rate, and take-off distance. The intersection of these constraints defines the acceptable region for wing loading and power loading. From this region, a wing loading value of 9 and a thrust-to-weight ratio of 1.62 are selected, ensuring that all performance requirements are satisfied simultaneously.

C. Wing and tail design

Using equation (7) and equation (8), the wing reference area $S = 4.0795181\ ft^2$ ($0.379\ m^2$) and power requirement $P = 0.734874\ HP$ ($547.99\ W$), respectively. The resulting wing design, with a mean aerodynamic chord ($\bar{C}$) of 229.642 mm. Figure 7 illustrates the reference geometry of the wing and horizontal stabilizer derived from the preliminary design calculations. The wing configuration is determined based on the selected wing loading and aerodynamic requirements, while the horizontal tail area is sized using the horizontal tail volume coefficient to ensure adequate longitudinal stability. This configuration establishes the baseline geometry required to balance lift generation and pitching moment control, forming the foundation for subsequent aerodynamic optimization. Obtained the horizontal stabilizer reference geometry, where $x_h = 0.602317\ m$ represents the horizontal tail arm length and $\bar{V}_h = 0.701188104$ denotes the horizontal tail volume coefficient, conducting equation (9), the projected area of the horizontal stabilizer s_h was calculated as $0.0860366\ m^2$.

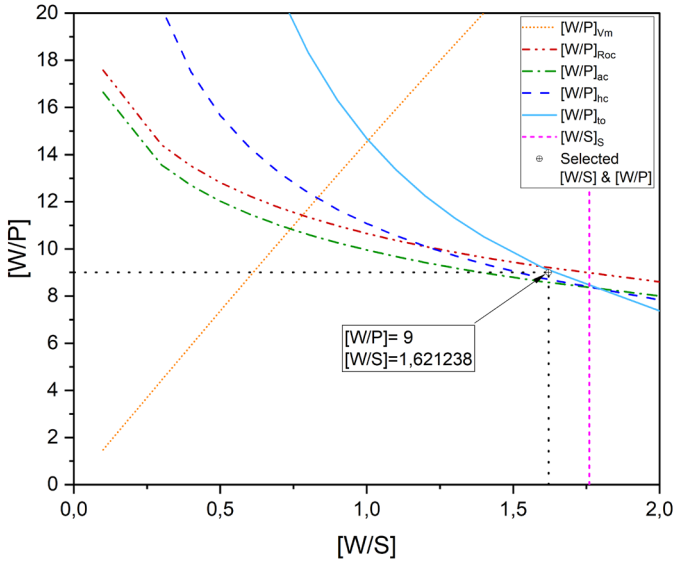

Figure 6. Matching plot.

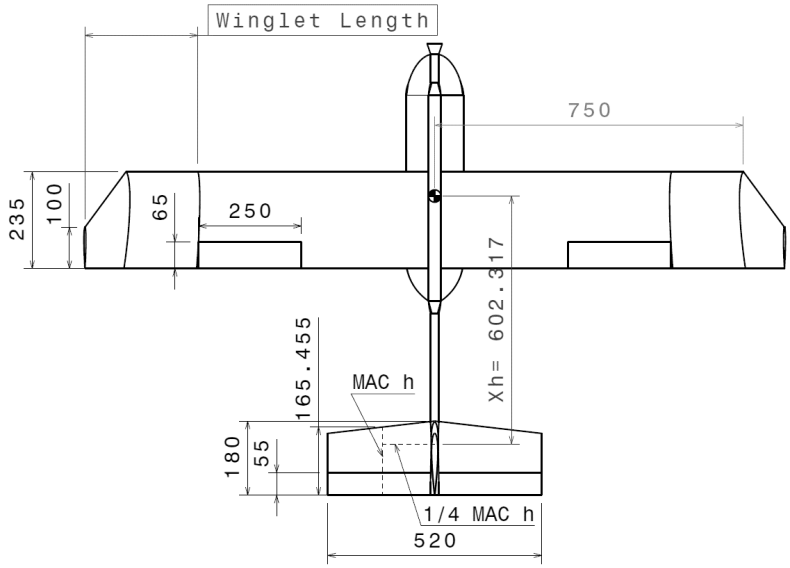

Figure 7. Wing and horizontal tail design.

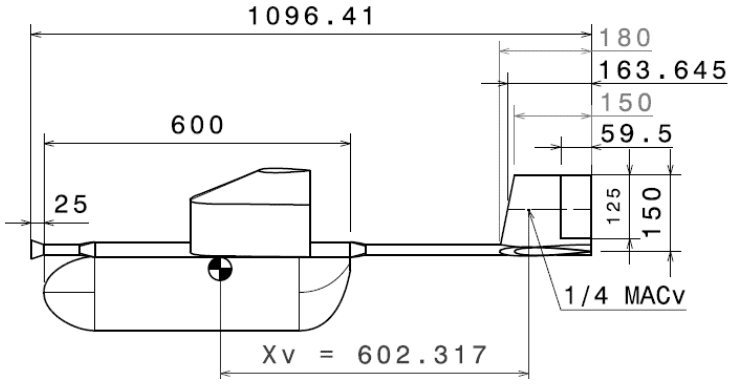

Figure 8. Vertical tail design.

Figure 8 describes the reference geometry of the vertical stabilizer with $x_v = 0.602317\ m$ and $\bar{V}_v = 0.220979152$. Using equation (10) to obtained horizontal stabilizer's projected area, Figure 8 presents the geometry of the vertical stabilizer, which is designed based on the vertical tail volume coefficient and tail arm length. The vertical tail plays a critical role in providing directional stability and controlling yawing motion. The selected configuration ensures sufficient restoring moment under sideslip conditions, contributing to the overall lateral-directional stability of the UAV. Obtained S_v is 0.024818 m^2.

D. Wing optimization

The UAV design defined in XFLR-5 is shown in Figure 9. The analysis was conducted using the Vortex Lattice Method 2 (VLM2) to obtain the values of C_L, C_D and V, T relative airspeed required for cruising conditions. Figure 4 the Clark-Y airfoil is used as a twistable or independent variable from wing section 1 to wing section 3, while wing section 4 uses the NACA 0010 airfoil with a fixed twist angle of 0°. The wing is symmetrical, and the chord length varies between sections 2 and 4 of the wing section along the Y-axis (lateral) direction.

Three independent variables, as shown in Table 2, were used for three responses. Response surface methodology was employed to produce the expected outcomes. Data was tested for normality and adequacy using normal plots for residuals and outliers, as analyzed by Design Expert software. Figure 10 shows the UAV model implemented in XFLR-5 for aerodynamic analysis using the Vortex Lattice Method (VLM). The geometry incorporates the defined wing configuration, airfoil distribution, and tail arrangement based on the preliminary design parameters. This model is used to evaluate aerodynamic characteristics such as lift, drag, and required airspeed under varying winglet configurations. The use of XFLR-5 enables efficient parametric analysis of multiple design variations, providing the dataset required for subsequent optimization using response surface methodology (RSM). Figure 10 (a) shows the C_L data points, Figure 10 (b) shows the C_D data points, and Figure 10 (c) shows the V data points. All data points exceeding the allowed range of ±3.62672 were considered abnormal. Data was obtained by conducting XFLR-5.

Figure 11 illustrates the response surface plots representing the interaction effects of winglet length, cant angle, and twist angle on lift coefficient, drag coefficient, and airspeed. The results demonstrate that the twist angle significantly influences lift generation, while the cant angle and winglet length affect both drag and aerodynamic efficiency. These interactions highlight the trade-offs between achieving higher lift

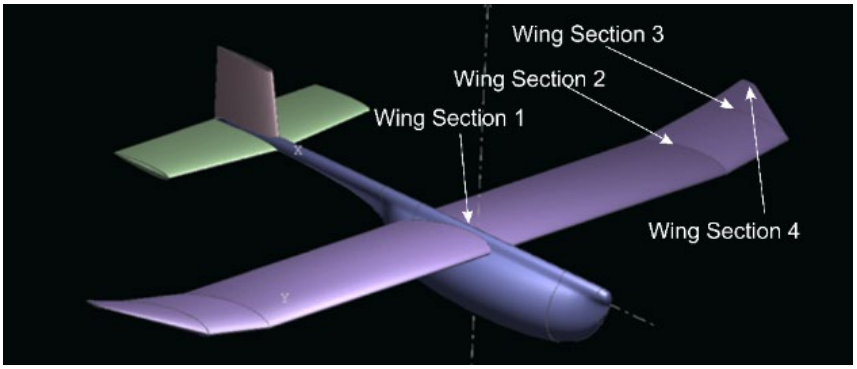

Figure 9. XFLR-5 plane design.

and maintaining low drag, emphasizing the importance of multi-variable optimization in UAV wing design. The response surface methodology was employed to optimize the wing geometry by varying independent variables to achieve the highest C_L, lowest C_D, and a target airspeed (V) of 16.8 m/s. In clean variables, which

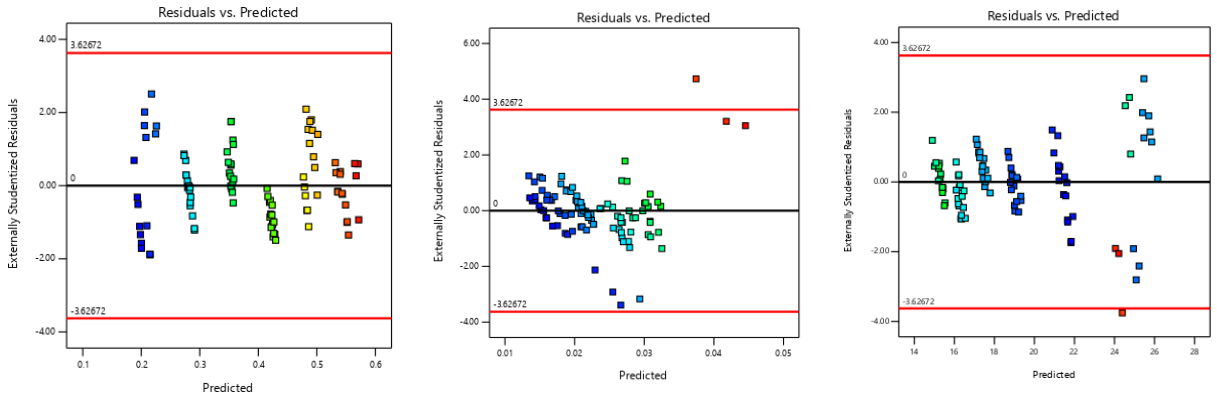

(a) (b) (c)

Figure 10. Outliner chart of (a) C_L; (b) C_D; (c) V.

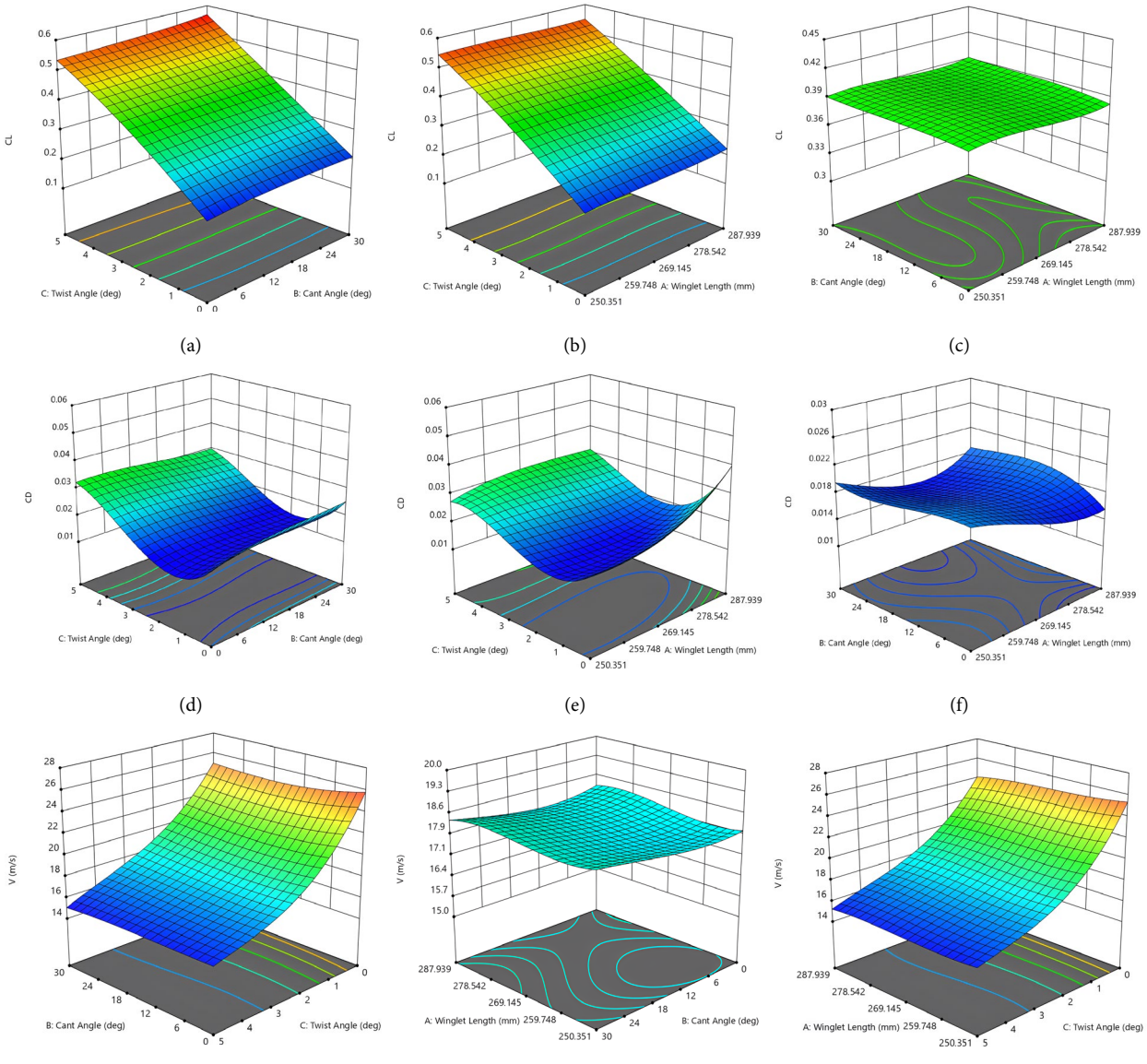

(a) (b) (c)

(d) (e) (f)

(g) (h) (i)

Figure 11. 3D Surface Contour Plot. (a) C_L affected by Twist and cant angle; (b) C_L affected by Twist and cant angle; (c) C_L affected by Twist and cant angle; (d) C_D affected by Twist and cant angle; (e) C_D affected by Twist and cant angle; (f) C_D affected by Twist and cant angle; (g) V affected by Twist and cant angle; (h) V affected by Twist and cant angle; (i) V affected by Twist and cant angle.

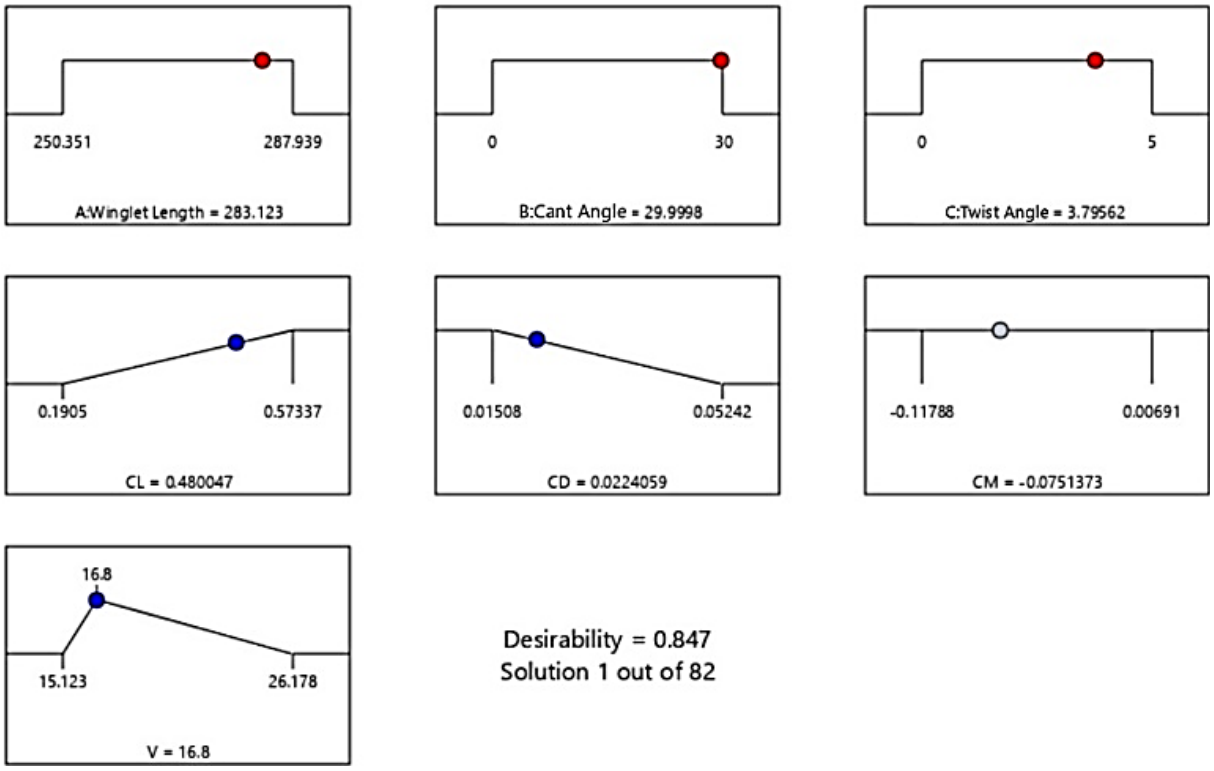

Figure 12. Optimal solution ramp.

have no winglet and twist angle, C_L is obtained at 0.19135, C_D is obtained at 0.02122, and V is required at 26.2 m/s.

Figure 12 presents the optimization results obtained using the response surface methodology, showing the optimal combination of design variables. The ramp function indicates that a winglet length of 283.123 mm, cant angle of approximately 30°, and twist angle of 3.8° yield the best performance. This configuration achieves the target cruising speed of 16.8 m/s while increasing the lift coefficient to approximately 0.48 and maintaining a relatively low drag coefficient. The result confirms the effectiveness of the optimization approach in meeting aerodynamic performance requirements.

E. Mass distribution

The UAV design is plotted in XFLR-5 according to the optimal solution ramp and tail references. The weight distribution is illustrated in Figure 13 and provided in Table 5. According to Table 5 and conducting equation (19) to equation (21), the CG location was found to be $\bar{x}_{CG} = 58.7\ mm$, $\bar{Y}_{CG} = 0\ mm$, and $\bar{Z}_{CG} = -33.93\ mm$.

Figure 13 illustrates the mass distribution of the UAV components used to determine the center of gravity location. The placement of major components such as the battery, motor, and payload is carefully arranged to achieve a center of gravity near 25 % of the mean aerodynamic chord. This configuration is critical to ensure stable flight characteristics and directly influences the aerodynamic moment and control effectiveness of the aircraft.

F. Static stability and trim analysis

Longitudinal stability is specified by $C_{M\alpha}$, $C_{M\alpha}$ based on the variation of δ_e at -4°, -2°, 0°, 2°, and 4°. Figure 14 shows the relationship between pitching moment coefficient and angle of attack for various elevator deflections. The negative slope of the curve indicates that the UAV satisfies the criteria for

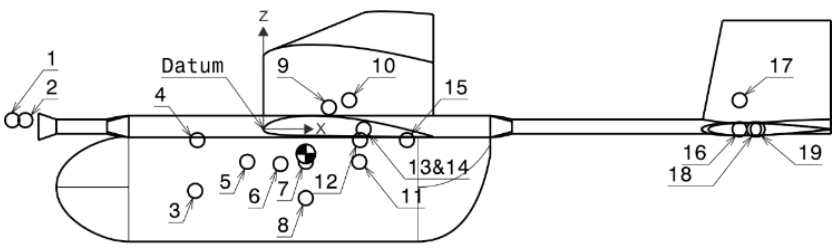

Figure 13. Mass distribution.

Table 5.
UAV components and mass distribution.

No	Item	Mass (g)	X (mm)	Y (mm)	Z (mm)
1	Propeller	23	-347.25	0	12.5
2	Motor	138	-329.25	0	12.5
3	Battery	606	-94.25	0	-85
4	ESC	70	-91.25	0	-15
5	Power module	20	-22.25	0	-45
6	fuselage	625	23.75	0	-48
7	Flight controller	38	58.75	0	-45
8	Camera	223	58.75	0	-95
9	GPS	32	58.75	0	30
10	Wing	953	118.75	0	0
11	Buzzer	5	132.75	0	-45
12	Receiver	15	133.75	0	-15
13	R Aileron servo	12	138.75	-380	0
14	L Aileron servo	12	138.75	380	0
15	Telemetry	24	198.75	0	-15
16	Rudder servo	12	658.75	0	0
17	Verstab	60	658.75	0	40
18	Elevator servo	12	678.75	0	0
19	Horstab	120	683.75	0	0
	Total	**3000**			

longitudinal static stability. This behavior confirms that the aircraft has an inherent tendency to return to its equilibrium condition after a pitch disturbance, which is essential for stable and controlled flight during aerial mapping missions. Using linear regression at $\delta_e = 0°$ the values obtained were $C_{M\alpha}$ = -0.0331 and $C_{M\delta_e}$ = -0.0273.

Lateral stability, as characterized by the yawing moment coefficient $C_{n\beta}$, $C_{n\beta}$ was analyzed at various rudder deflections δ_r at -6°, -4°, -2°, 0°, 2°, 4°, and 6°. Figure 15 presents the variation of the yawing moment coefficient with respect to the sideslip angle under different rudder deflections. The positive slope of the curve indicates that the UAV exhibits directional static stability. This means the aircraft can generate a restoring yawing moment when subjected to lateral disturbances, ensuring stable flight behavior in crosswind conditions. Linear regression analysis at $\delta_r = 0°$ yielded a $C_{n\beta}$ = 0.0002 and rudder control power $C_{n\delta_r}$ = -0.0012.

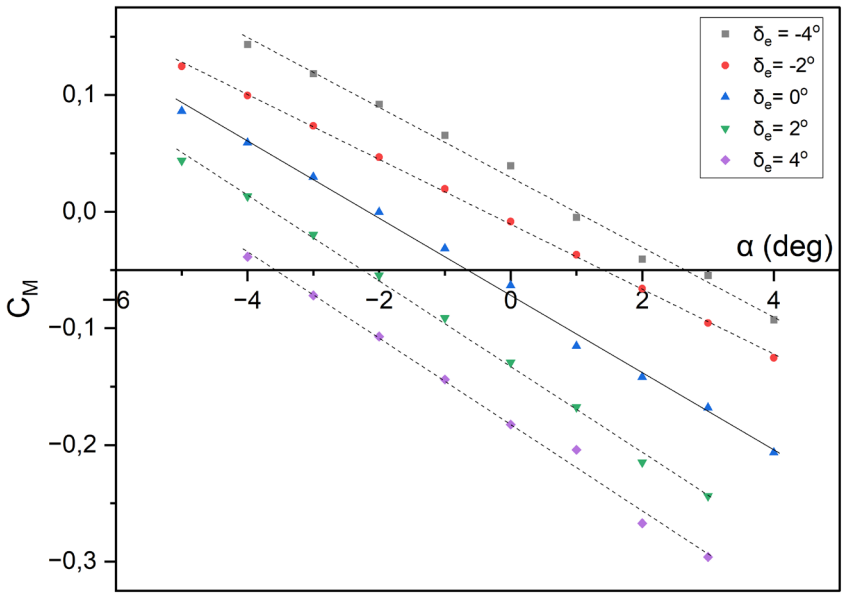

Figure 14. $C_{M\alpha}$ at δ_e variation.

δ_r at -6°, -4°, -2°, 0°, 2°, 4°, and 6° also affects roll moment coefficient. Figure 16 illustrates the influence of rudder deflection on the rolling moment coefficient. The results indicate that rudder input not only affects yawing motion but also contributes to rolling behavior due to aerodynamic coupling effects. This interaction highlights the importance of considering control surface coupling in the stability and control analysis of UAV configurations. obtained that $C_{l\delta_r} = 6 \times 10^{-5}$

Roll stability, characterized by the rolling moment coefficient $C_{l\beta}$ was analyzed. Figure 17 shows the relationship between the rolling moment coefficient and the sideslip angle, which is used to evaluate lateral stability. The observed trend indicates that the UAV generates a restoring rolling moment when subjected to sideslip, confirming its lateral static stability. This characteristic is essential to maintain wing-level flight and ensure a predictable response to disturbances, the relationship between C_l and sideslip angle (β), yielded a $C_{l\beta}$ value of -0.0036.

Figure 18 presents the effect of aileron deflection on the rolling moment coefficient, representing the control power of the aileron. The results show a consistent change in rolling moment with respect to control input, indicating effective roll control authority. This confirms that the aileron configuration is sufficient to provide the required maneuverability and control responsiveness for the UAV. The aileron control power ($C_{l\delta_a}$) was determined to be -0.0034.

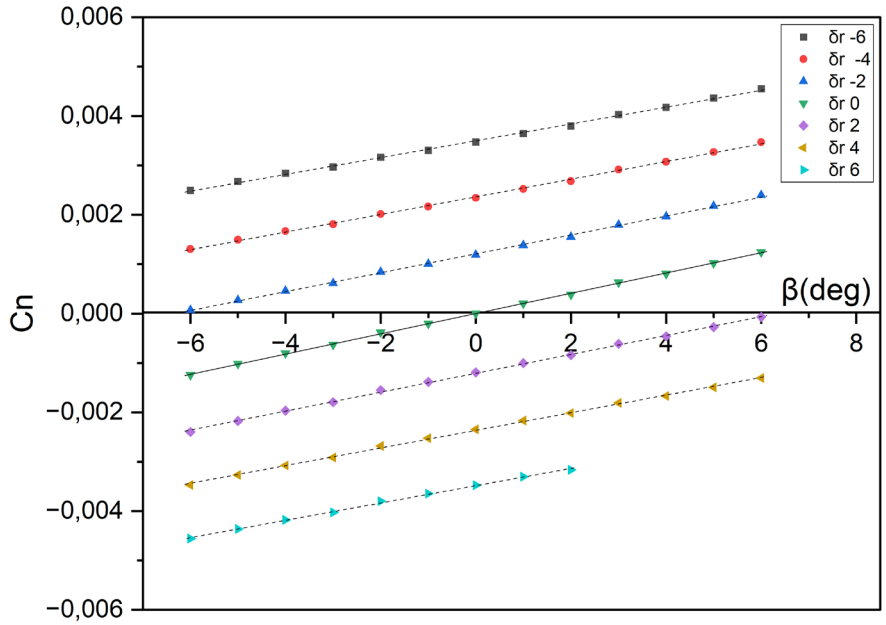

Figure 15. $C_{n\beta}$ at δ_r variation.

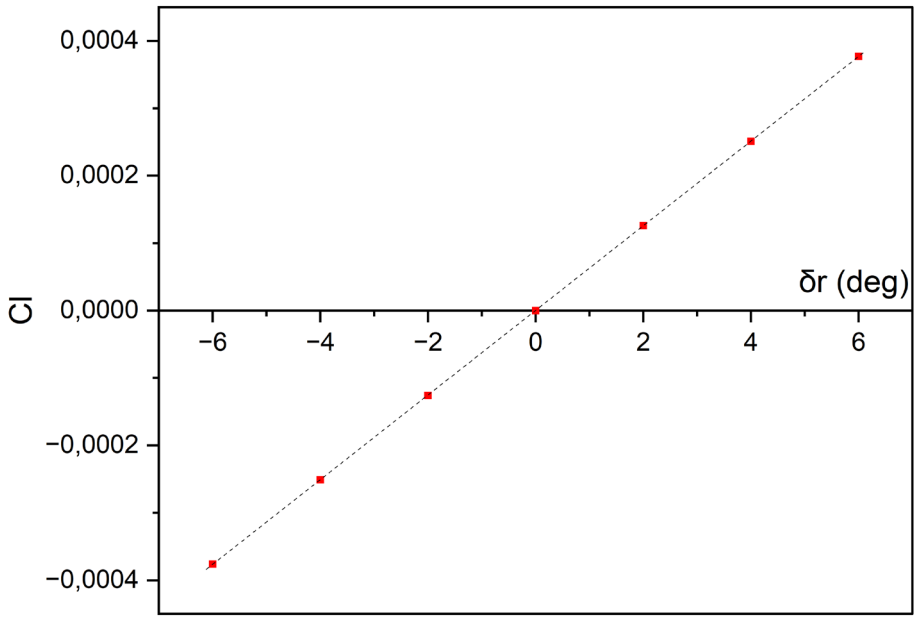

Figure 16. δ_r affect C_l .

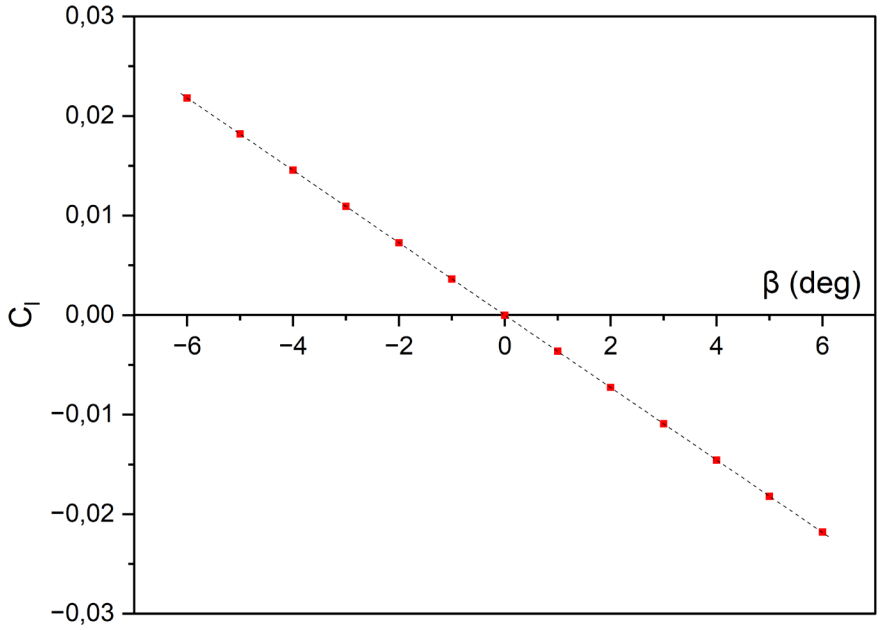

Figure 17. C_l at β variation.

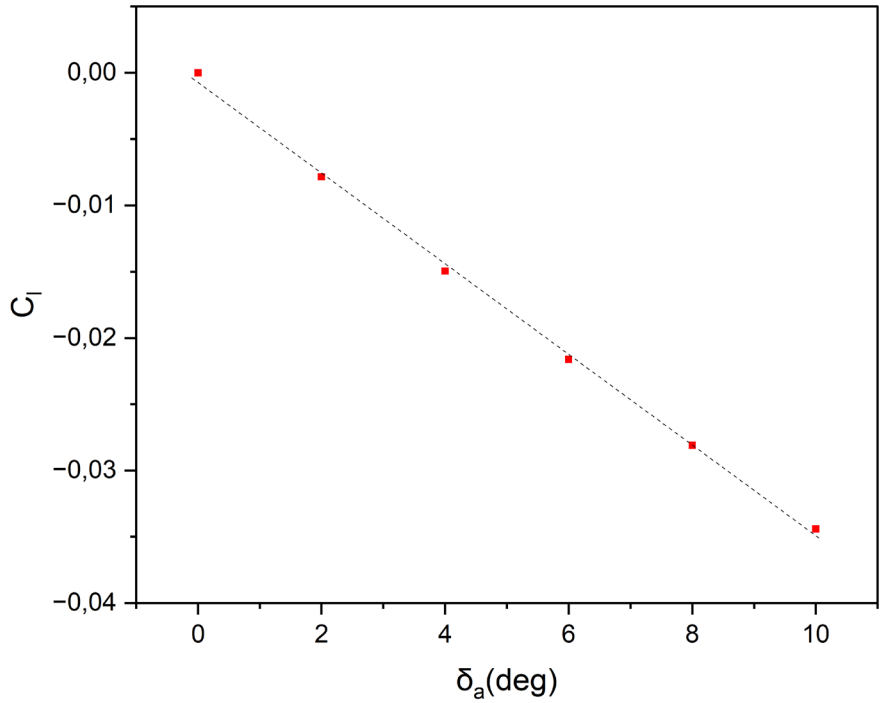

Figure 18. C_l at δ_a variation.

IV. Conclusion

This study aims to optimize the preliminary design of a fixed-wing unmanned aerial vehicle (UAV) for aerial mapping applications by improving aerodynamic performance and ensuring static stability through wing geometry optimization. The results demonstrate that the integration of conceptual and preliminary design methods with aerodynamic simulation using XFLR-5 and optimization through response surface methodology (RSM) successfully identified an optimal wing configuration. The optimized design achieved the target cruising speed of 16.8 m/s, with an improved lift coefficient of approximately 0.48 and a controlled drag coefficient of approximately 0.022. Furthermore, static stability analysis confirmed that the UAV satisfies longitudinal, lateral, and directional stability criteria under various control surface deflections. The findings highlight the effectiveness of combining aerodynamic simulation with statistical optimization techniques to systematically explore the design and improve UAV performance. This approach provided a computationally efficient alternative to high-fidelity

methods while still delivering reliable design insights, making it particularly suitable for early-stage UAV development. Future work should focus on incorporating structural and aeroelastic effects into the optimization framework, as well as conducting experimental validation through real flight testing. Additionally, further research can explore multi-objective optimization approaches to simultaneously consider aerodynamic performance, structural weight, and energy efficiency for more comprehensive UAV design improvements.

Declarations

Author contribution

P.V. Lesalli: Writing - Original Draft, Conceptualization, Formal analysis, Investigation, Visualization, Data Curation. **T.P. Soemardi**: Conceptualization, Writing - Review & Editing, Resources, Software, Visualization, Funding acquisition, Supervision. **L. Mariani**: Writing - Review & Editing, Conceptualization, Investigation, Validation.

Funding statement

This research has been funded under LPDP Lembaga Pengelola Dana Pendidikan (Indonesian Endowment Fund for Education Agency).

Competing interest

The authors declare that they have no known competing financial interests or personal relationships that could have appeared to influence the work reported in this paper.

The use of AI or AI-assisted technologies

The authors did not use AI or AI-assisted technologies in any part of the preparation of this manuscript.

Additional information

Reprints and permission: information is available at https://mev.brin.go.id/.

Publisher's Note: National Research and Innovation Agency (BRIN) remains neutral with regard to jurisdictional claims in published maps and institutional affiliations.

References

[1] A. M. Samad, N. Kamarulzaman, M. A. Hamdani, T. A. Mastor, and K. A. Hashim, "The potential of unmanned aerial vehicle (UAV) for civilian and mapping application," presented at *the 2013 IEEE 3rd International Conference on System Engineering and Technology*, Shah Alam, Malaysia, 2013.

[2] P. P. R. Aidil, Liyantono, and M. Solahudin, "Multi-copter development as a tool to determine the fertility of rice plants in the vegetation phase using aerial photos," *Procedia Environmental Sciences,* vol. 24, pp. 258-265, 2015.

[3] M. A. Boon, A. P. Drijfhout, and S. Tesfamichael, "Comparison of a fixed-wing and multi-rotor UAV for environmental mapping applications: A case study," *The International Archives of the Photogrammetry, Remote Sensing and Spatial Information Sciences,* vol. XLII-2/W6, pp. 47-54, 2017.

[4] P. E. Kaparos, C. D. Bliamis, and K. Yakinthos, "Conceptual design of a UAV with VTOL characteristics," presented at the AIAA Aviation 2019 Forum, 2019.

[5] M. H. Sadraey, *Design of Unmanned Aerial Systems* (Aerospace Series). Manchester, NH, USA: John Wiley & Sons, 2020.

[6] Federal Aviation Administration (FAA), Aircraft Weight and Balance Handbook: FAA-H-8083-1A. Skyhorse Publishing Inc., 2011.

[7] P. V. Lesalli, "Preliminary design dan analisis weight and ballance surveillance mapping UAV tricopter V-TOL tilt rottor 2 meter wing span," in *Prosiding Seminar Nasional Teknologi Informasi dan Kedirgantaraan : Peran Generasi Z dalam Dunia Kedirgantaraan*, Yogyakarta, 2022.

[8] S. Kakade, D. Chikkala, K. Reghunath, and A. Seeni, "Aerodynamic analysis and optimization of wings for the jain university sailplane using XFLR5," *ECS Transactions,* pp. 493-513, 2022.

[9] R. C. Nelson, *Flight stability and automatic control.* New York: WCB/McGraw Hill, 1998.

[10] Munyak, Nathen Evan, "Evaluation of XFLR5 for predicting stability and dynamics of a ready-to-fly trainer aircraft," Honors Capstone Projects and Theses, 158, 2020.

[11] M. Prieto, M. S. Escarti-Guillem, and S. Hoyas, "Aerodynamic optimization of a VTOL drone using winglets," *Results in Engineering,* vol. 17, 2023.

[12] K. Anuar, M. Akbar, and Herisiswanto, "Wing design of UAV serindit v-1," *IOP Conference Series: Materials Science and Engineering,* vol. 539, no. 1, 2019.

[13] P. V. Lesalli and M. A. Cahyono, "Longitudinal static stability analysis with wing swept angle variation Of UAV flying wing surveillance adelaar 2 use software XFLR 5," (in Indonesia), *Conference SENATIK STT Adisutjipto Yogyakarta,* vol. 6, 2020.

[14] İ. H. Güzelbey, Y. Eraslan, and M. H. Doğru, "Numerical investigation of different airfoils at low Reynolds number in terms of aerodynamic performance of sailplanes by using XFLR5," vol. 8, no. 1, pp. 47-65, 2018.

[15] A. Septiyana *et al.*, "Static stability analysis on twin tail boom UAV using numerical method," presented at The 8th International Seminar on Aerospace Science and Technology – ISAST 2020.

[16] A. Septiyana *et al.*, "Analysis of aerodynamic characteristics using the vortex lattice method on twin tail boom unmanned aircraft," presented at The 7th International Seminar on Aerospace Science and Technology – ISAST 2019.

[17] A. Jankovic, G. Chaudhary, and F. Goia, "Designing the design of experiments (DOE) – An investigation on the influence of different factorial designs on the characterization of complex systems," *Energy and Buildings,* vol. 250, 2021.

[18] S. Nagaraju, P. Vasantharaja, N. Chandrasekhar, M. Vasudevan, and T. Jayakumar, "Optimization of welding process parameters for 9Cr-1Mo Steel using RSM and GA," *Materials and Manufacturing Processes,* vol. 31, no. 3, pp. 319-327, 2015.

[19] P. Sahoo, "Optimization of turning parameters for surface roughness using RSM and GA," *Advances in Production Engineering & Management,* vol. 6.3, pp. 197-208, 2011.

[20] M. Hafid, J. Istiyanto, and N. Nasruddin, "Multiobjective optimization of dimension and position of elliptical crush initiator on crashworthiness performance of square tube using response surface methodology," *Frontiers in Mechanical Engineering,* vol. 9, 2023.

[21] A. A. G. Hanif, H. S. Li, M. A. Raza, M. Kamran, and M. Abdullah, "Optimization design of an aircraft wing structure based on response surface method," *IOP Conference Series: Materials Science and Engineering,* vol. 887, no. 1, 2020.

[22] X. Yao, W. Liu, W. Han, G. Li, and Q. Ma, "Development of response surface model of endurance time and structural parameter optimization for a tailsitter UAV," *Sensors (Basel),* vol. 20, no. 6, Mar 22 2020.

[23] A. K. Kundu, M. A. Price, and D. Riordan, *Conceptual aircraft design: An industrial approach*. John Wiley & Sons, 2019.

[24] A. K. Kundu, M. A. Price, D. Riordan, P. Belobaba, J. Cooper, and A. Seabridge, *Theory and practice of aircraft performance*. John Wiley & Sons, 2016.

[25] A. Karki, K. Darlami, and S. Bhattrai, "Conceptual design and stability analysis of a fixed wing uas research platform for aerial experiments," in *Proceedings of 10th IOE Graduate Conference*, 2021, pp. 35-41.

[26] J.-M. Moschetta and K. Namuduri, "Introduction to UAV systems," in *UAV Networks and Communications*, 2017, pp. 1-25.

[27] A. P. P. Rizky, Liyantono, and M. Solahudin, "Analysis of aerial photo for estimating tree numbers in oil palm plantation," *IOP Conference Series: Earth and Environmental Science,* vol. 284, no. 1, 2019.

[28] C. R. Victor Antonio and S. Yan, "Preliminary design and performance-stability analysis of a fixed-wing UAV using XFLR5," *Journal of Aircraft and Spacecraft Technology,* vol. 7, no. 1, pp. 8-16, 2023.

[29] M. Zambare, A. Pardeshi, A. Pingle, and R. Ansari, "Design and analysis of fixed wing unmanned aerial vehicle," *International Journal of Innovative Science and Research Technology (IJISRT),* pp. 1630-1637, 2024.

[30] J. Roskam, *Airplane design part V component weight estimation*. Lawrence: DARcorporation, 2018.

[31] J. Roskam, *Airplane design*. United States: DARcorporation, 1985.

[32] D. Raymer, *Aircraft design: A conceptual approach, Sixth Edition*. American Institute of Aeronautics and Astronautics, Inc., 2018.

[33] P. Dutta, O. P. Nagar, S. K. Sahu, R. R. Savale, and R. Gokul Raj, "Aerodynamic analysis of bionic winglet-slotted wings," *Materials Today: Proceedings,* vol. 62, pp. 6701-6707, 2022.

[34] P. Panagiotou, S. Antoniou, and K. Yakinthos, "Cant angle morphing winglets investigation for the enhancement of the aerodynamic, stability and performance characteristics of a tactical blended-wing-body UAV," *Aerospace Science and Technology,* vol. 123, 2022.

[35] S. Kolappan, I. Neethi Manickam, K. Robinston Jeyasingh Swikker, S. Joe Patrick Gnanaraj, and M. Appadurai, "Performance analysis of aircraft composite winglet," *Materials Today: Proceedings,* vol. 62, pp. 889-895, 2022.

[36] M. Jaeger and D. Adair, "Conceptual design of a high-endurance hybrid electric unmanned aerial vehicle," *Materials Today: Proceedings,* vol. 4, no. 3, pp. 4458-4468, 2017.

[37] P. C. Wang, J. H. Shih, C.-Y. Chen, and K. B. Lua, "Effects of propeller size and position on the performance of a UAV wing in a distributed propulsion system," vol. 38, no. 5, p. 04025055, 2025.

[38] S. Carroll, J. Satme, S. Alkharusi, N. Vitzilaios, A. Downey, and D. Rizos, "Drone-based vibration monitoring and assessment of structures," *Applied Sciences,* vol. 11, no. 18, 2021.

[39] S. I. Gonzalez-Cabrera, N. Camacho-Zamora, S. R. Rojas-Ramirez, A. M. Gonzalez-Aguilar, M. O. Vigueras-Zuniga, and M. E. Tejeda-Del-Cueto, "Structural vibration analysis of UAVs under ground engine test conditions," *Sensors (Basel),* vol. 26, no. 2, Jan 15 2026.

[40] A. J. Keane, A. Sóbester, and J. P. Scanlan, *Small unmanned fixed-wing aircraft design: A practical approach*. John Wiley & Sons, 2017.